GEOPHYSICS, VOL. 81, NO. 3 (MAY-JUNE 2016); P. P47–P60, 25 FIGS.
10.1190/GEO2015-0305.1

Reducing high-frequency ghost cavitation signals from marine air-gun arrays

Martin Landrø[1], Yuan Ni[2], and Lasse Amundsen[3]

ABSTRACT

Ghost cavitation, which is a term describing that cavitation bubbles are generated acoustically, has been hypothesized to occur when the ghost reflected signals from many individual air guns beneath the sea surface produce a pressure that is close to zero in the water above the source array. Ghost cavitation is typically observed some milliseconds after the ghost reflection, and it may last for 5–15 ms, depending on the configuration of the source array. The cavitation process subsequently generates a weak high-frequency signal. To investigate this potential signal model and mechanism, we have performed a dedicated source experiment. We found that the distance between the source strings in a source array is a major factor that influences the amount and strength of the high-frequency signal. By increasing the separation distance from 6.5 to 8 m, we have observed a significant decrease in the high-frequency signal. Further, the amount of ghost cavitation can be reduced by increasing the distance between the guns. Also single sub-arrays may create ghost cavitation sound, of course weaker in signal strength compared with full arrays, in agreement with the model. Conventional air-gun modeling can be used to predict where ghost cavitation can occur. Therefore, in principle, a workflow could be developed to quantify grossly if and how much high-frequency signals could be generated by this mechanism, given the source array configuration, and further change the configuration to reduce to a very minimum the high-frequency signals, if deemed necessary. For an air-gun array consisting of two subarrays separated by 6 m and fired at 9 m depth, we found that the high-frequency signals emitted between 1 and 10 kHz were of similar strength to the noise from conventional cargo ships, depending on their size and the vessels' speed.

INTRODUCTION

The use of near-field measurements measuring the acoustic signal at a distance of approximately 1 m from each air gun in a marine air-gun array is proposed and demonstrated by Ziolkowski et al. (1982), and it is later improved by Parkes et al. (1984). Landrø et al. (1991) test the method on compact air-gun arrays and find that the near- to far-field method produces instable results in this case. Later, Landrø (2000) suggests that when air guns are placed close together, the total pressure in the water (close to and above the air guns) might approach zero, meaning that cavitation might occur. The explanation for this is that when several ghost signals (with negative dynamic pressure) add together, the resulting pressure in the water might approach zero. If the near-field hydrophone is located in an area where cavitation could occur, nonlinear effects consequently will also occur, and thus the extrapolation to the far field will be less valid. Landrø et al. (2011) present measurements that indicate that this indeed might actually occur, and suggest to use the term ghost cavitation for this. Later on, the repeatability properties of this ghost cavitation signal were studied (Landrø et al., 2013). In this paper, we will focus mainly on high-frequency signals created by the ghost cavitation effects. Other effects that may generate high-frequency signals are phenomena related to the release of air in individual air guns, such as clicks from the solenoid, cavities formed close to the air gun, and jumping of the guns. These effects are discussed in more detail in Landrø et al. (2011).

The experiment used in the two previous papers (Landrø et al., 2011, 2013) was not designed to confirm that ghost cavitation

Manuscript received by the Editor 9 June 2015; revised manuscript received 12 November 2015; published online 06 April 2016.
[1]Norwegian University of Science and Technology (NTNU), Department of Petroleum Engineering and Applied Geophysics, Trondheim, Norway. E-mail: martin.landro@ntnu.no.
[2]CGG, Massy, Paris, France. E-mail: yuan.ni@cgg.com.
[3]Norwegian University of Science and Technology (NTNU) and Statoil Research Centre, Trondheim, Norway. E-mail: lasse.amundsen@ntnu.no.

actually is a cause for high-frequency signals generated by compact marine air-gun arrays. Therefore, in this paper, we present results from a dedicated test in which we investigate if ghost cavitation occurs, and finally how we can use this knowledge to reduce this signal if needed.

Recently, Coste et al. (2014) presented a new air gun specially designed to reduce the high-frequency emission. They show that the primary peak from the new gun is less sharp and therefore contains fewer high frequencies compared with a conventional air gun. Using near- to far-field simulation, they find that the new source should be capable of reducing the emitted signals by approximately 10 dB for the frequency range between 100 Hz and 10 kHz. More than 10 kHz, this difference is less pronounced. To some extent, this new source is expected to reduce the amount of ghost cavitation because the primary peak is reduced somewhat. For near-field recordings, they find that the primary peak is reduced from 3.9 to 3.0 bar-m, corresponding to a 23% decrease. Nevertheless, it is also important to be aware of the ghost cavitation effect, which is more coupled to how we design and operate our marine air-gun source arrays, and not to the design of the individual guns.

The growing interest in high-frequency emission from marine air-gun arrays is mainly driven by environmental concerns. We know that marine mammals and fish have hearing curves that extend well above the seismic frequencies (0–100 Hz) and up to 200 kHz. Some studies of the high-frequency sound from air-gun arrays are Goold and Fish (1998) and Breitzke et al. (2008). Amundsen and Landrø (2010), review and plot hearing curves of marine mammals. Southall et al. (2007) present a comprehensive review on marine mammal hearing and suggest criteria for when various behavioural effects might occur. Laws (2012) uses the work of Southall et al. (2007) to estimate the extent of hearing damage zones around a seismic source. Groenaas et al. (2011) present a new system for detection of whales during seismic acquisition. The purpose of this paper is to present results from a dedicated experiment focusing on ghost cavitation sound, and to suggest some ways to attenuate this signal.

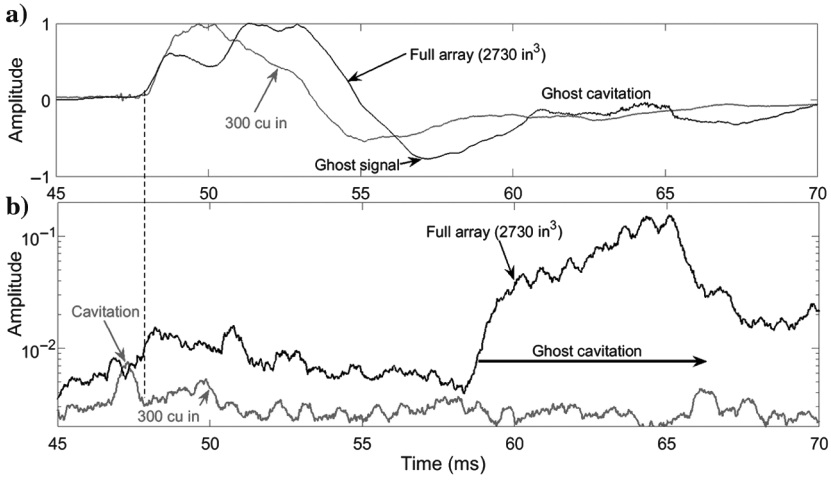

Figure 1. (a) Recorded far-field signals of full array (black) and a 300 in^3 single air gun (gray). The data have been normalized prior to plotting (the maximum amplitude of the full array is 8.3 times that of the single gun). (b) The same data after applying a 30 kHz high-pass filter, absolute value, and smoothing. Notice that cavitation signals are observed prior to the main peak for the single gun (marked by arrow) and after the ghost signal for the full array, denoted as ghost cavitation. The ghost cavitation signal is approximately 10 times stronger than the high-frequency signal observed approximately 50 ms for the full array.

BACKGROUND AND MOTIVATION FOR A DEDICATED GHOST CAVITATION EXPERIMENT

Figure 1 shows data from the experiment discussed in Landrø et al. (2011). For details on acquisition and analysis, we refer to that paper. Figure 1a shows a comparison between the recorded signals at the seabed approximately 60 m below a large air-gun array (2730 in^3) and a single 300 in^3 air gun. In the upper plot, the two signals have been normalized to one to ease the comparison. For the full array (black line), we notice that the primary peak is wider (48–55 ms) than for the single gun (48–53 ms), which we attribute to variations in firing time delays and sizes in gun volumes for the large array. This causes a corresponding shift of 1–2 ms in the minimum for the ghost signals that occur at 55 ms for the single gun and 56.5 ms for the full array. Approximately at 58 ms, we observe the start of a high-frequency signal for the full array, lasting for approximately 7 ms. This is what we interpret as the ghost cavitation signal. Figure 1b shows that after a 30 kHz high-pass filter, this signal is significantly stronger for the full array than for the single gun. Actually, there is no such high-frequency signal for the single gun in the corresponding time span (after the ghost signal). Landrø et al. (2011) suggest that this high-frequency signal is caused by cavities created by the collective ghost reflections from multiple air guns. Because this signal is not observed for the single gun, it is likely for us to assume that the signal is caused by some kind of interaction, or the fact that the air guns are relatively close together in a regular air-gun array. To test the validity of this ghost cavitation hypothesis, we decided to perform a dedicated experiment in which the distance between the subarrays in an air-gun array is changed. If the high-frequency signal observed after the ghost reflection is caused by ghost cavitation, we should expect that the strength and amount of this cavitation signal should decrease if the distance between air guns is increased. We also observe that there is a high-frequency signal associated with the air escaping from the air-gun ports (marked by an arrow in the lower plot in Figure 1). We think that this signal is attributed to collapses of small cavities close to the air-gun ports. Furthermore, we think that these cavities are created by rapid water movements close to the air gun, similar to cavities collapsing at propellers. In addition to the acoustic experiments, we also decided to acquire high-speed photos by mounting a camera at one of the gun strings.

THE FIELD EXPERIMENT

The field test was performed offshore Congo in 2011. The shooting vessel was the *M/V Princess*, and several configurations of the source array were tested. The weather conditions were good (calm seas) during the experiment. The water depth varied between 1500 and 3000 m for the test, and the vessel speed was less than 2 knots. The high-frequency data were recorded by a hydrophone suspended at 17 m below the source array. It should be noted that there is an uncertainty related to the actual position of the hydrophone because there will always be some deviations due to towing effects. The hydrophone sampling rate is 0.00192 ms, which gives a Nyquist frequency of approximately 260 kHz. The source array con-

sisted of two subarrays, as shown in Figure 2. All air guns in the source array are G-Gun II. The minimum time between shots was 10 s. Source depths of 6 and 9 m were tested, as well as increasing the crossline separation distance between the two subarrays from 6.5 to 8 m. Some tests in which the two subarrays were displaced by 10 and 20 m were also conducted. Unfortunately, the first peak and the corresponding ghost (strongest signals) of the signal were saturated or clipped on most recordings. However, the high-frequency signal, which is our main focus here, is retained for many of the experiments, and those measurements are the ones that have been used. Our main argument for assuming that the data recorded after the peak and ghost signals are valid for this analysis is that they appear similar to previous unclipped data (shown in Figure 1 and discussed in previous papers [Landrø et al., 2011, 2013]).

The recording system includes an EA-SDA14 recorder (24-bit Sigma Delta) working at 312.5 kS/s, with four calibrated channels (±0, 1 dB), and each channel is connected with a HTI-99-HF hydrophone, with a frequency response from 2 Hz (−3 dB) to 125 kHz (−3 dB). The sensitivity of the HTI-99-HF hydrophone is 204 dB re 1 V/μPa. No gain was applied on the hydrophones. The clipping occurred at ±0.5 V. We had planned to place the hydrophones at a much deeper position and calculated the necessary hydrophone sensitivity. However, during the test, the hydrophones stayed at a shallower depth, and this caused the saturated peak signals.

GHOST CAVITATION VERSUS SOURCE SEPARATION DISTANCE

The existence of ghost cavitation as proposed by Landrø et al. (2011) has not been proven so far. It might be difficult to do so, but one way to establish this theory is to simply increase the crossline spacing between the two subarrays in an air-gun array. We should then expect that the amount of ghost cavitation signals (high-frequency signals) should decrease, simply because the acoustic energy of the ghost signals in the area between the two subarrays will be less, and that the potential area in which cavitation might occur will be reduced. Figure 3 shows the recorded signals for two different subarray separation distances: 6.5 and 8 m. We notice that the signals are saturated at the maximum peak (shown as dashed lines at the top of the figure) and that the signal corresponding to the closest separation distance is more saturated than the other. Because the ghost cavitation signal is expected to arrive 6–20 ms (see Landrø et al., 2013) after the primary peak, we think that the ghost cavitation signal is not heavily influenced by this saturation effect. We observe that the ghost cavitation signal is saturated for times between 44.7 and 45.2 ms for a 6.5 m separation distance. The effect of this saturation effect is minor when a 10 kHz high-pass filter is applied to the data, as shown in Figure 4. There are two key observations that can be made from Figure 4: The amplitude of the high-frequency signal is reduced for the larger separation distance. Furthermore, we also observe that there is a time delay of approximately 1 ms between the 6.5 and 8 m separation distances. To investigate this issue in more detail, we performed a simple source modeling study using the method described in Ziolkowski (1970). The modeling example (not identical to the experiment, but very similar, so it is used for the purpose of illustrating the effect) in Figure 5 confirms these observations: The time window for when cavity production is possible is shifted and reduced in length as the separation distance is increased. Another similarity that is striking between Figures 5 and 3 is that the width of the peak signal (although saturated in Figure 3) increases as the separation distance increases. In Figure 5, all modeled values that are below the green straight line correspond to negative absolute pressure, which of course is unphysical. It simply means that the linear assumption that we use when we superimpose the signal from each individual air gun in the array is breaking down. In reality, when nonlinear effects are included, these pressure values will approach zero, and therefore we will assume that when this occurs for the linear model, this is an indication that cavity production might occur. Furthermore, we also observe that the actual level of negative pressure decreases with separation distance. A more realistic modeling for the actual configuration used in the field experiment is presented in Figure 6, where we observe a 3D version of the "cavity cloud" surrounding the gun array. In this figure, we have used conventional air-gun modeling (Ziolkowski, 1970) to estimate volumes in the water column, in which the modeled pressure is below a certain threshold. There are also source modeling approaches for generator injector guns (Landrø, 1992) and water guns (Landrø et al., 1993)

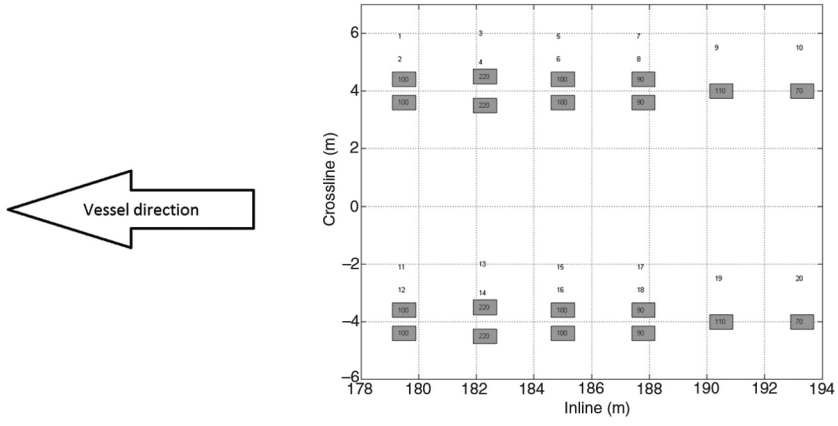

Figure 2. Configuration of the source array. The port and starboard subarrays are identical with a volume of 1200 in^3 (19.7 l). The volume of the full array is 2400 in^3 (39.3 l).

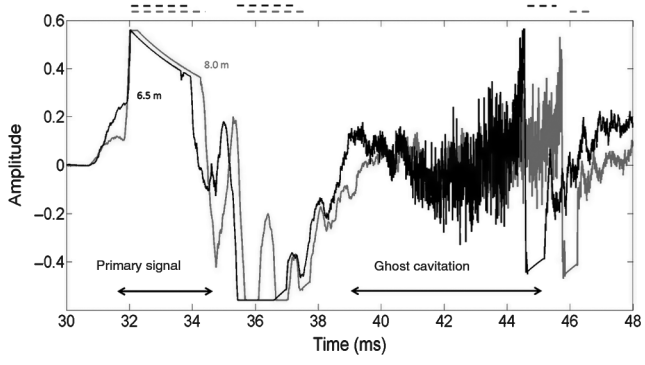

Figure 3. Signals measured at the hydrophone at a 17 m depth for full source using a crossline separation distance of 6.5 m (solid black line) and for a crossline separation distance of 8 m (solid gray line). The source depth is 9 m, and the dashed black and gray lines at the top indicate when the recorded signal is saturated. The amplitude units are volts. Multiplication by 0.106 converts the data into bar.

available. In the current modeling example, we have used a threshold value of −0.1 bar. We observe that after 14.5 ms (Figure 6a), a cavity cloud is formed above the center of the array (midway between the two subarrays and above them); 2 ms later (Figure 6b), this cloud has increased significantly, covering approximately half of the available volume above the air-gun array. The shape is ellipsoidal, and it is likely for us to assume that at this time a lot of cavities are formed (above the array). After 18.5 ms, the cavity cloud has decreased in volume and also descended below the array, and finally after 19.5 ms, the cavity cloud is small, and it will disappear within the next millisecond. This means that according to this 3D modeling example, the time window for cavity production is approximately 7 ms. A similar modeling example is shown in Figure 7 for the case in which the separation distance between the two subarrays is increased to 9 m. We observe essentially the same cycle as described for Figure 6; however, in this case, the size of the cavity cloud is smaller, simply due to the increased separation distance. Hence, we expect more ghost cavitation for the closest separation distance, and this is exactly what we observe in Figure 4.

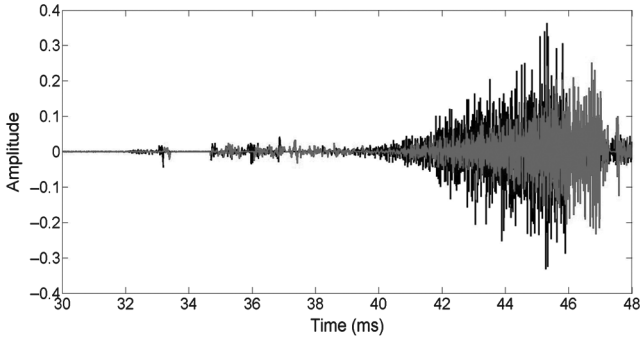

Figure 4. The same signatures as in the previous figure, after application of a 10 kHz high-pass filter. Black and gray represent separation distances of 6.5 and 8 m, respectively. We observe that the amount of high-frequency signal decreases with separation distance and that the envelope of the high frequency (HF) signal is delayed by approximately 1 ms. Amplitude units are arbitrary.

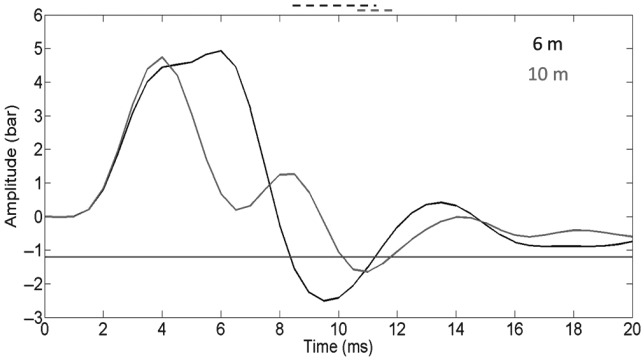

Figure 5. Modeling the effect of increasing the source separation distance: Black line represents the signal modeled at 2 m depth midway between two subarrays deployed with a crossline separation of 6 m. Gray line represents signal modeled at 2 m depth when the separation distance is increased to 10 m. The expected time window for cavity creation is shown by dashed black and red lines. The horizontal line indicates the level for zero hydrostatic pressure (equal to the negative value of the hydrostatic pressure).

Figure 8 shows a smoothed version of Figure 4, after taking the absolute values first, then smoothing each trace, followed by stacking 16 shots. The time window in which the ghost cavitation signal is saturated, is shown as gray and light-red rectangles for subarray crossline separations of 6.5 and 8 m, respectively. These rectangles might vary slightly for different shots, and here we have shown those corresponding to the shot shown in Figure 4. This gives a clearer impression of the amplitude levels of the high-frequency signal for the two separation distances: The maximum high-frequency level is reduced by approximately 23% (1.3–1.0) by increasing the separation distance by 1.5 m. We also observe that the high-frequency signal from the wider array is delayed by approximately 0.7 ms compared with the close separation case. This is in qualitative agreement with the modeling example shown in Figure 5, where a time delay of 1.6 ms is observed. The subarray distance is increased from 6.5 to 8 m in the field test (Figure 8) and from 6 to 10 m in the modeled example shown in Figure 5, which explains why the time shift is somewhat larger for the modeled case. If only the port array is fired (blue line in Figure 8), we notice that the corresponding amount of ghost cavitation signal is significantly weaker and shorter in duration. This corresponds to increasing the crossline separation distance to infinity.

If we apply a 130 kHz high-cut filter to the data, this difference is more pronounced, as shown in Figure 9. When comparing Figures 8 and 9, we notice that the amplitude level decreases by a factor of approximately 6 for the closest separation distance. For the wider array (8 m separation distance), the same ratio is approximately 8.

In this context, it is useful to introduce the cavitation number (see, for instance, Ceccio and Brennen, 1991):

$$\sigma = \frac{P - P_V}{\frac{1}{2}\rho U^2}, \tag{1}$$

where P is the water pressure, P_v is the water vapor pressure, ρ is the water density, and U is the water velocity. Ceccio and Brennen (1991) perform cavity experiments using a low-turbulence water tunnel to generate cavities, and they find a slightly larger difference between cavitation values (σ) equal to 0.45 and 0.55 at 130 kHz compared with 10 kHz (Figure 21 in their paper). In our case (where the cavitation is caused by the ghost signal), a narrow source array will generate a lower water pressure than a wider array, which fits with the observed difference between the 10 and 130 kHz case for the two array configurations. Figure 10 shows amplitude spectra for the two array configurations (narrow and wide), and we clearly observe that the difference is increasing with increasing frequency. This increase is not as evident in Ceccio and Brennen (1991).

Finally, the existence of high-frequency signals more than 130 kHz strongly supports the idea that this signal is mainly caused by cavitation.

GHOST CAVITATION FROM SINGLE SUBARRAYS

According to the ghost cavitation theory (Landrø et al., 2011), it should also be possible to create ghost cavitation from a single subarray given that the total ghost signal is above a certain threshold. This is probably the case, as is shown in Figures 11 and 12. The level of this signal is approximately nine times weaker than the corresponding high-frequency signal from the full array using a 6.5 m separation distance (Figure 8; solid blue line). Furthermore, we notice from these figures that when the source depth is reduced,

there is only a minimal increase in the strength of the cavitation signal. However, the timing of the deeper source is shifted by approximately 1.8 ms (after aligning the two measurements at the primary peak). This corresponds roughly to the traveltime difference between the two source depths, which is 2 ms (assuming 3 m difference and 1500 m/s sound velocity). This indicates that the area or volume where cavity creation occurs is practically the same for the two cases, maybe with slightly less volume for the deeper source because the ghost signal is expected to be weaker then. If this high-frequency sound is created by bubble motion close to the air guns, we should not have observed a delay like this; then the two high-frequency signal bursts should have been aligned (when the primary peaks are aligned, as in our case).

It is somewhat surprising that the amplitude difference between the two curves in Figure 12 is not larger, because the ghost amplitude difference should be of the order of 30%–40% due to the difference in source depth between the two experiments (assuming that the ghost cavity cloud is at approximately the same depth). In Figure 13, we have plotted the eight individual shots in the same manner as in Figure 12, and we clearly observe that the deeper source gives more stable results. The weather conditions did not change significantly between the 9 and 6 m experiments. We notice from

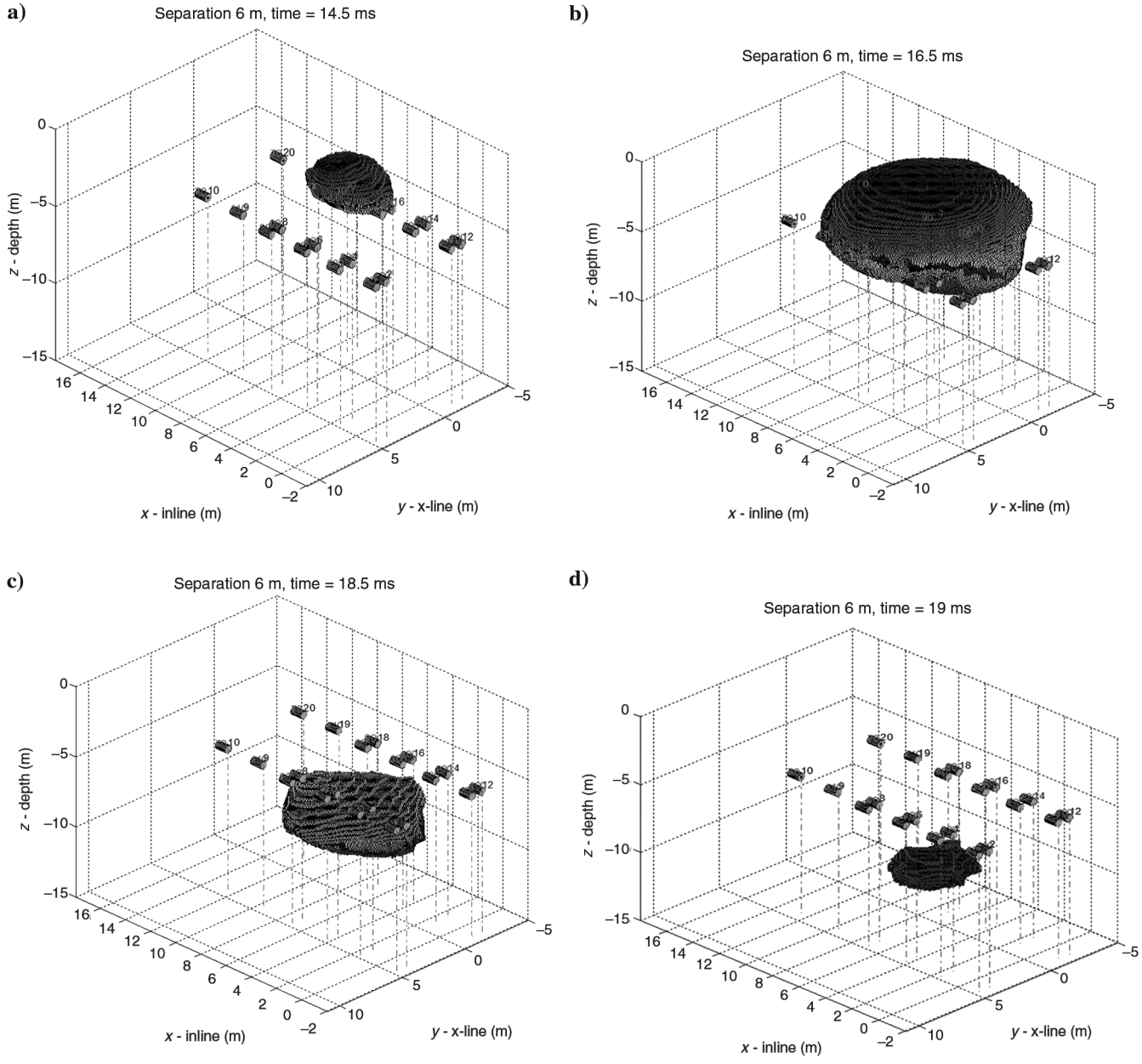

Figure 6. (a-d) Modeled volumes for cavity creation for 14.5, 16.5, 18.5, and 19.5 ms for a substring separation distance of 6 m. We have assumed that cavity creation occurs if the modeled pressure is less than −0.1 bar. We notice that the maximum cavitation volume occurs at 16.5 ms, is located above the gun array, and descends with time.

Figure 13 that some of the individual signals actually produce an amplitude level that is higher than the corresponding signals from the deeper source, as expected. Comparing photos (Figure 14) taken at the two days (but not necessarily at exactly the same time) for the two experiments, we observe only small changes in the sea state. According to the observers' log, the swell size was approximately 2 m for both experiments. If we assume that the sea surface has a sinusoidal shape, the ghost reflections will be focused and defocused due to the shape of the surface. According to Aizenberg et al. (2008), this curvature effect might be modeled using the effective reflection coefficient concept. This effective reflection coefficient depends on the parameter R^*:

$$R^* = \frac{R_S}{1 - \kappa R_S}. \tag{2}$$

Here, we have assumed an incidence angle of zero, R_S is the distance from the source to the curved interface (in our case, equal to the source depth), and κ is the curvature of the sea surface. Figure 15 shows R^* as a function of source depths for $\kappa = 1/2$ m^{-1} and $\kappa = 1/3$ m^{-1}. We notice that the absolute value of R^* is larger for shallower source depths and that the difference increases as the curvature decreases. Such focusing and defocusing effects are therefore expected to be stronger for shallower source depths. This might lead to increased cavitation activity (if the ghost signals are focused) or

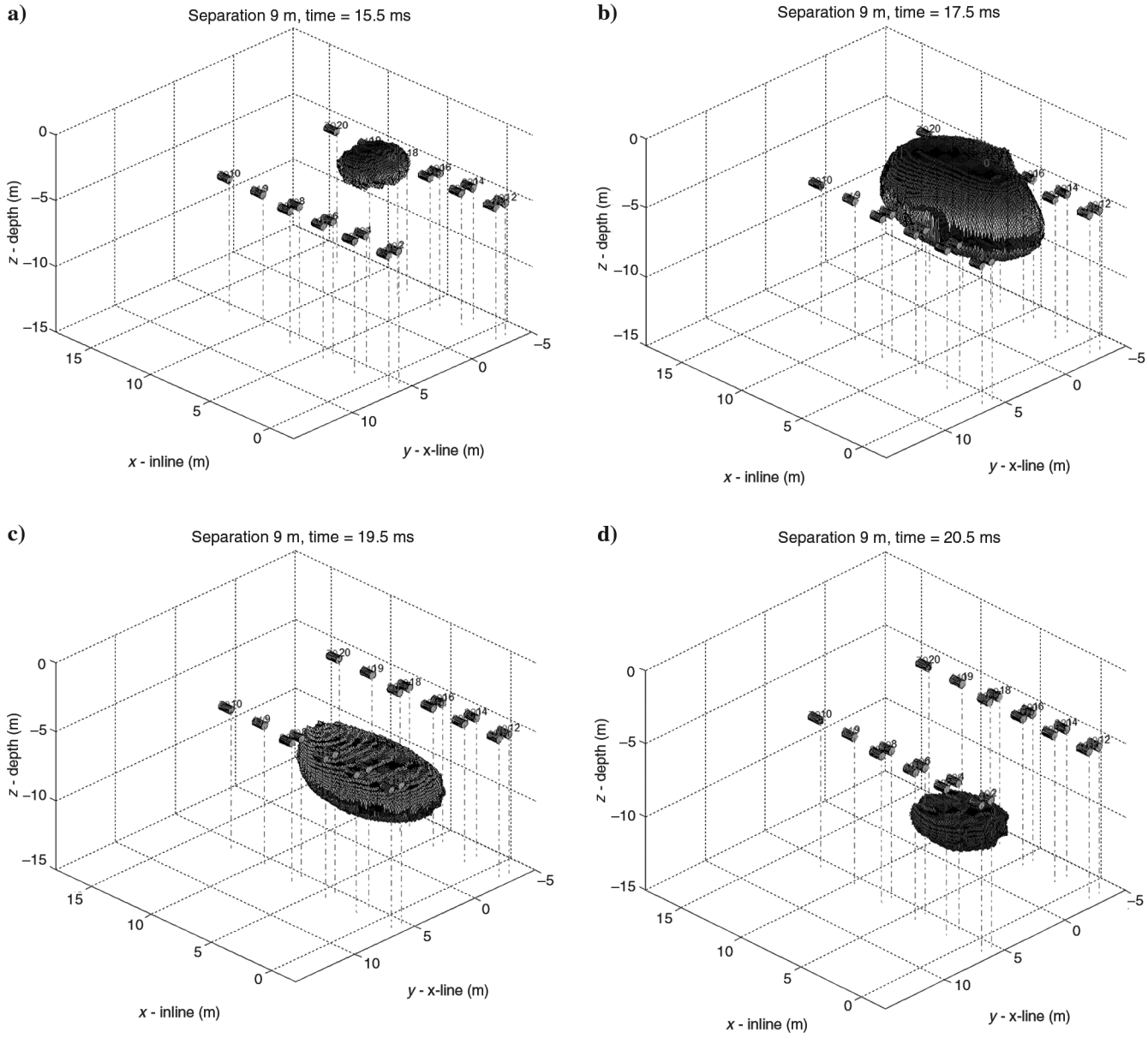

Figure 7. (a-d) Modeled volumes for cavity creation for 14.5, 16.5, 18.5, and 19.5 ms for a substring separation distance of 9 m. We have assumed that cavity creation occurs if the modeled pressure is less than −0.1 bar. We notice that the maximum cavitation volume occurs at 16.5 ms, is located above the gun array, and descends with time.

decreased cavitation activity (if the ghost signals are defocused). The combined effect of focusing and defocusing might explain why the 6 m data are less repeatable compared with the 9 m data. However, on average, we expect focusing to appear as much as defocusing, and therefore if we include more shots into our stacked high-frequency signal, there should be a difference between the 6 and 9 m source depths, because the average ghost signals are stronger for the shallow source depth. In a second run, we therefore increased the number of shots to be stacked from 8 to 16, and then the difference between the 6 and 9 m data is significant (almost a factor of 2), as shown in Figure 16. This means that the shape of the sea surface influences the ghost cavitation signal, but on average, a shallower source depth generates more ghost cavitation than a deeper source depth.

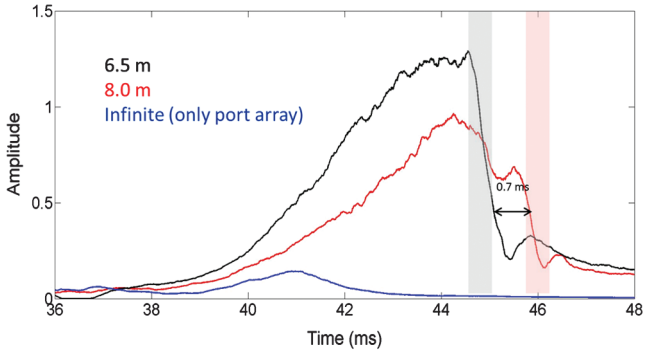

Figure 8. The absolute value and smoothing of the signals are shown in Figure 3. Black and red curves correspond to 6.5 and 8 m subarray separation distance, respectively. Notice that the maximum high-frequency signal is reduced by a factor close to 4. A 10 kHz high-pass filter has been applied to the data prior to the absolute value and smoothing, and 16 succeeding shots have been stacked for each case. The blue curve shows the same type or response for the case in which only the port array is fired at a 9 m depth. The gray and light red boxes show where the signal has been saturated (see Figure 3) for the 6.5 and 8 m data, respectively.

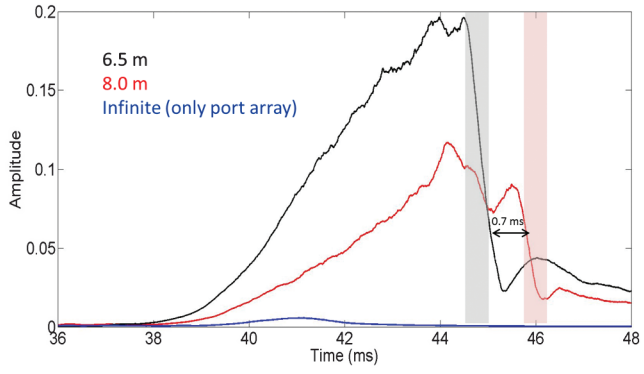

Figure 9. The absolute value and smoothing of the signals shown in Figure 3. The black and red curves correspond to 6.5 and 8 m subarray separation distance, respectively. A 130 kHz high-pass filter has been applied to the data prior to the absolute value and smoothing. Notice that the difference in this case is slightly larger than for a 10 kHz high-pass filter. The blue curve shows the same type or response for the case in which only the port array is fired at a 9 m depth. The gray and light red boxes show where the signal has been saturated (see Figure 3) for the 6.5 and 8 m data, respectively.

When we use air-gun modeling to estimate cavity clouds surrounding the single subarray, we find no clouds in this case. This means that there is a mismatch between our interpretation given above and the air-gun modeling. If we use a cut-off value of

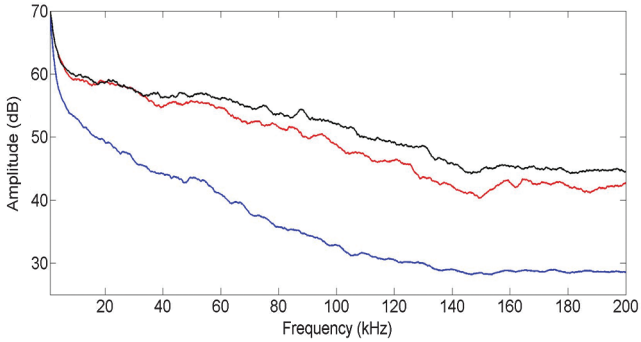

Figure 10. Amplitude spectra of a full array with 6.5 m subarray separation (black line) and 8 m spacing (red line). The port array only is shown in blue. The source depth is 9 m, and five spectra were stacked and then smoothed for this plot. Notice that the difference between the narrow and wider array configurations increases with frequency and that the difference is even larger for the port array only (blue). Amplitude values are arbitrary.

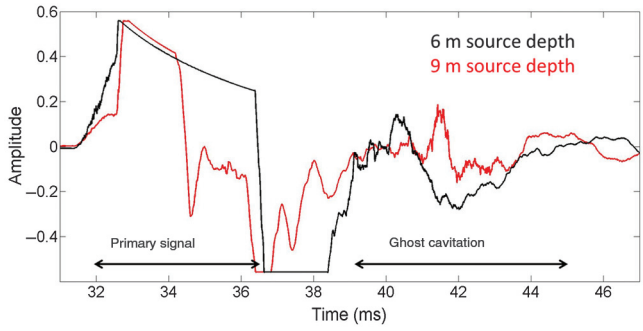

Figure 11. Signals measured at the hydrophone at 17 m depth for a single subarray (port array) for source depths of 6 (black) and 9 m (red), respectively. The units along the amplitude axis should be multiplied with 0.106 to convert into bar.

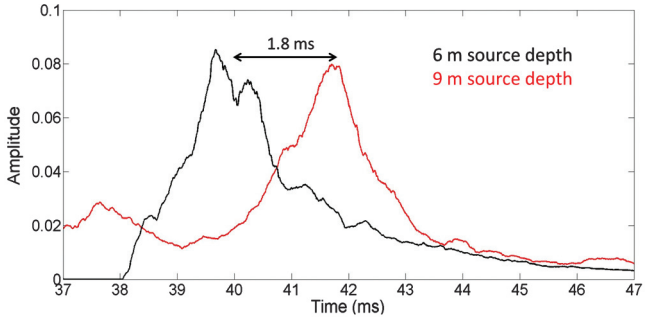

Figure 12. Amplitude stacks (after 10 kHz high-pass filter, absolute value, and smoothing) for eight shots when a single subarray (port array) is fired at 6 (black) and 9 m (red) source depth. Both signals are aligned at the primary peak (Figure 10). Notice the time shift of approximately 1.8 ms between the two high-frequency signals. The amplitude axis units are arbitrary.

0.2 bar as an example (instead of −0.1 bar as used previously), we observe clouds corresponding to volumes in which the absolute pressure in the water is less than 0.2 bar (Figure 17). This could either indicate that ghost cavitation might occur also for pressure values above the water vapor pressure or that air-gun modeling underestimates the effect. We believe that the latter is most likely. Air-gun modeling software is calibrated for frequencies between 5 and 250 Hz. It is therefore likely that the high-frequency response of air-gun modeling is not very accurate, and hence the maximum peak of each individual air gun might be slightly lower than in reality. Hence, a cut-off value of 0.2 bar might actually correspond to a cut-off value closer to zero.

Finally, we point out that the experiment of using only one subarray actually corresponds to an infinite separation distance (between subarrays). We can therefore assume that we have three measurements for how the high-frequency signal varies with separation distance: 6.5, 8 m, and infinite. These observations might be fitted to an exponential decay curve as shown in Figure 18, where the single string results are shown as dashed asymptotes for the exponential decay assumption. It is important to note that an exponential decay is an educated guess, and it is not based on a proper physical consideration. However, Figure 18 summarizes two of the main experimental results so far in a simple way: Increasing the separation distance between the subarrays in an air-gun source

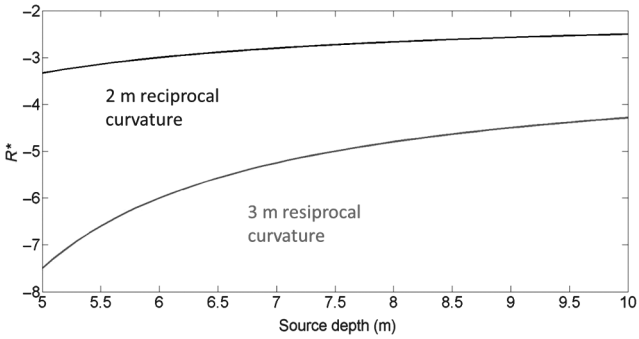

Figure 15. The effect of curvature on the ghost reflection amplitude: $R*$ versus source depth assuming a reciprocal curvature of 2 (black line) and 3 m (gray line), respectively. The absolute value of $R*$ (which is a measure of "focusing strength" increases with decreasing source depth.

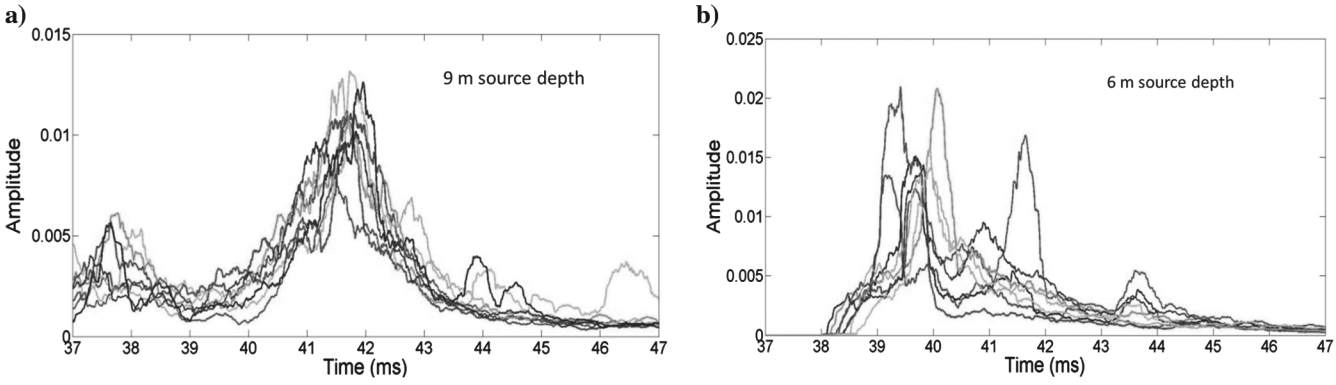

Figure 13. Individual amplitude plots (after a 10 kHz high pass, absolute value, and smoothing) of the eight shots used to obtain the stacked signals shown in Figure 11 for (a) 9 m source depth and (b) 6 m source depth. Only the port array is fired. Notice that the ghost cavitation signal (a) from the deep source is more stable than that (b) from the shallow source. This is probably caused by the changing weather conditions between the two experiments. The units along the amplitude axis are arbitrary.

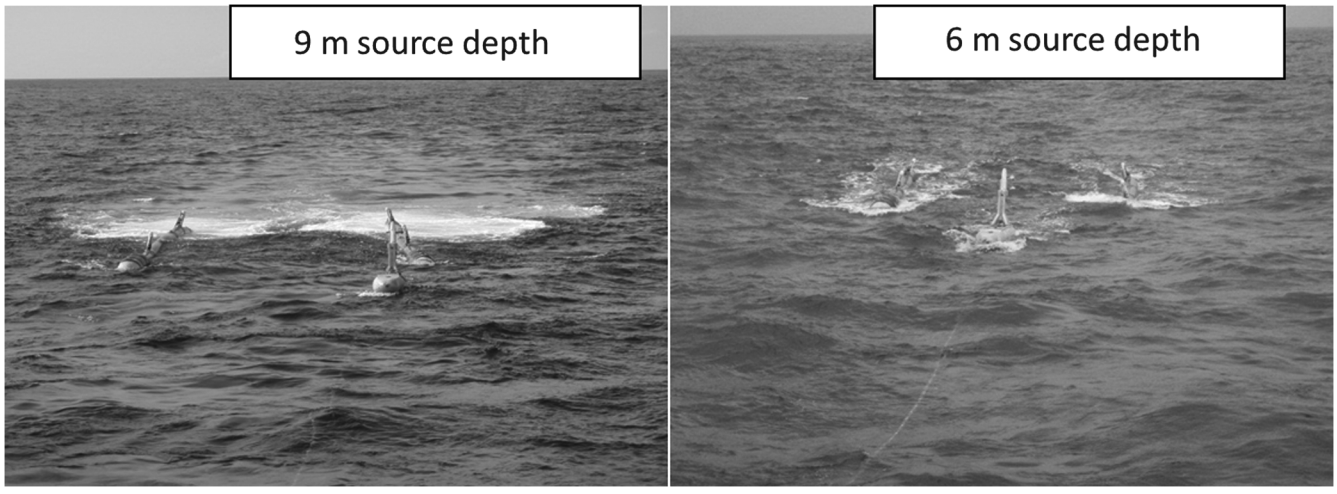

Figure 14. The sea state comparison between the two experiments is done at (left) 9 and (right) 6 m.

array reduces the amount of high-frequency signal significantly, and the decay is more rapid for higher frequencies.

ATTENUATING GHOST CAVITATION BY FIRING EXTRA GUNS

One way to try to counteract the ghost cavitation is to fire one or several air guns at a delayed time. This delay time should be optimized, so that the signal produced exactly counteracts the negative pressure signal as shown in, for instance, Figure 5. According to this figure, a good choice for the firing time delay could be 6–7 ms. From Figure 3, we notice that the delay time between the primary peak and the onset of the ghost cavitation signal is approximately 8 ms. In the field experiment, we delayed two guns in the array by 11 ms, and the resulting amplitude behaviour is shown in Figure 19. We observe that the two signals are very similar until 46 ms, where the signal corresponding to the experiment with two delayed air guns suddenly drops, whereas the full-array signal continues to increase in strength. This corresponds roughly to our expectations: The delayed air-gun signals counteract the ghost signals created by the majority of the guns in the source array, and the primary signals from these air guns counteract the ghost signals almost perfectly after 46 ms. Unfortunately, we did not test a shorter time delay, so we do not know for sure if we could actually attenuate more of the cavitation signal by using shorter time delays. Figure 19 only suggests that this is the case. It is however important to remember that the width of the primary signal for a single air gun is limited, typically 1–3 ms (depending on the frequency content). Because the total duration of the cavitation sound is typically longer than this (5–10 ms), it might be a good idea to use several guns with different time delays to attenuate this signal. It is evident from this example,

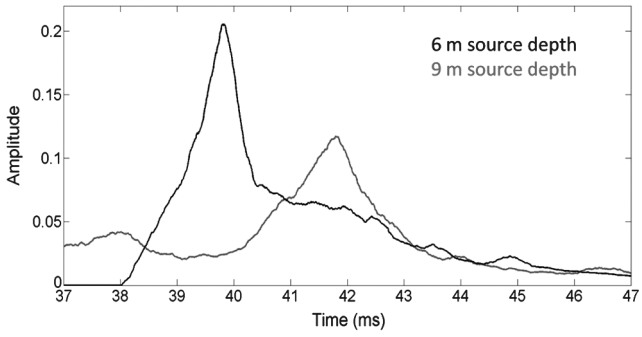

Figure 16. Amplitude stacks (after 10 kHz high-pass filter, absolute value, and smoothing) for 16 shots when a single subarray (port array) is fired at 6 (black) and 9 m (red) source depth. Both signals are aligned at the primary peak (Figure 10). The amplitude axis units are arbitrary.

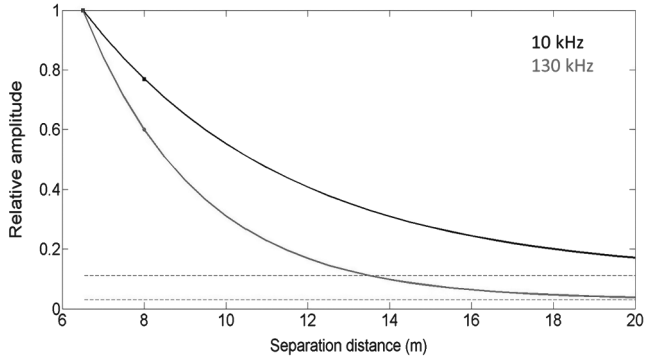

Figure 18. Amplitude variation of HF signal as a function of the separation distance between the two subarrays assuming exponential decay for 10 kHz high-pass filter (black) and 130 kHz high-pass filter (gray). The dashed lines represent relative amplitude levels for only one subarray (corresponding to infinite separation distance). The black squares and gray circles represent measured values for the two cases.

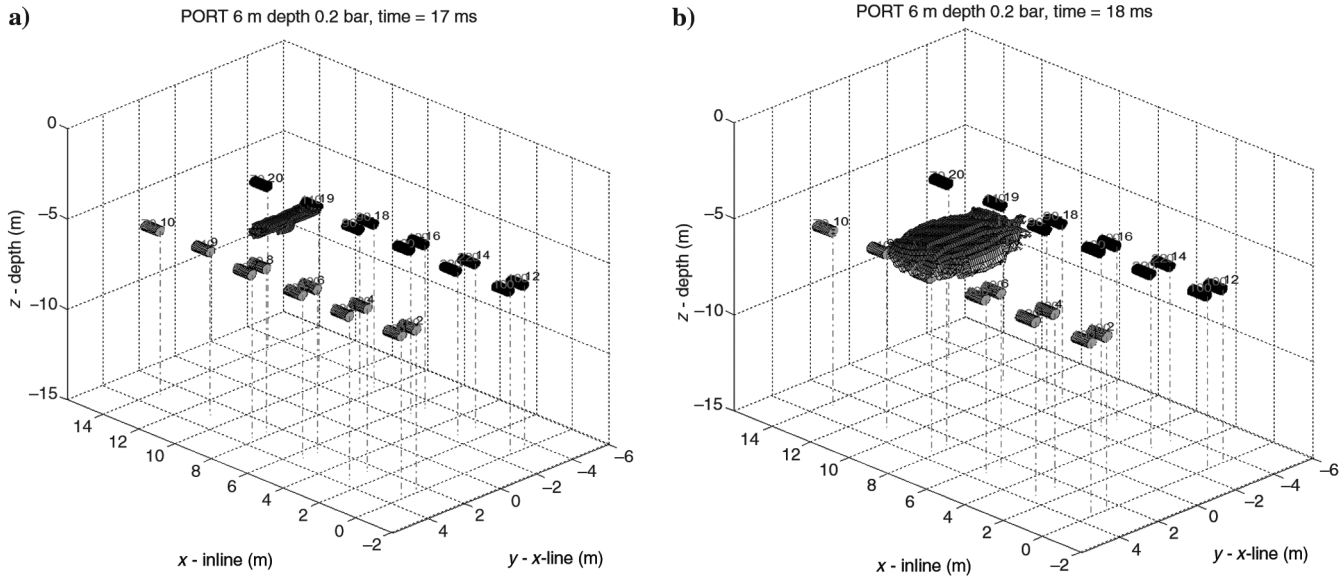

Figure 17. Modeled volumes for "cavity creation" for (a) 17 and (b) 18 ms when only the port array is fired at 6 m depth. In this, the cut-off level for cavity creation is set to 0.2 bar, which means that the purpose of the figure is to show that the modeled pressure is low in some areas above the array, but not as low as zero, according to the air-gun modeling.

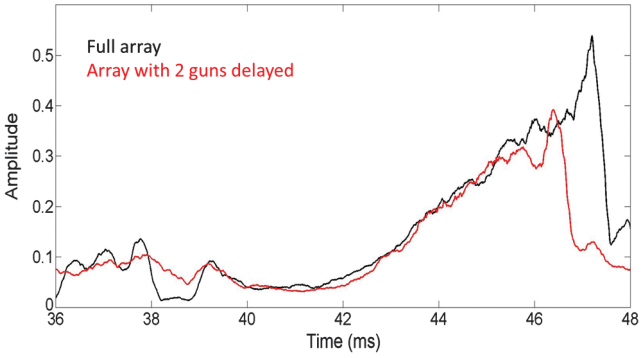

Figure 19. Amplitude stacks (after 10 kHz high-pass filter, absolute value, and smoothing) for eight shots for the full array (black line) and eight shots, where two individual guns were delayed by 11 ms (red line). Amplitude axis units are arbitrary.

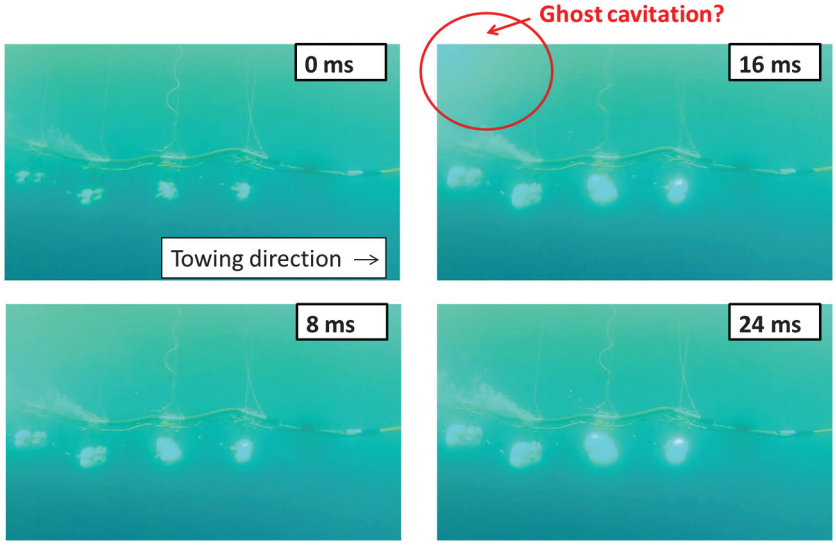

Figure 20. High-speed photos of one subarray for four different time instants after the source has been fired. We notice a "cloud" appearing after 8 ms that maximizes at approximately 16 ms and disappears again after 24 ms. This corresponds roughly to our acoustic observations of ghost cavitation.

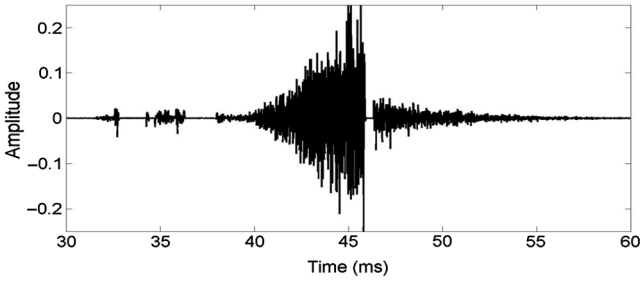

Figure 21. Recorded signal from the full array fired at 9 m depth with a subarray separation distance of 6.5 m. The data have been filtered with a 10 kHz high-pass filter. Notice that the full length of the ghost cavitation signal is approximately 15 ms (from 40 to 55 ms). The primary peak is at 32 ms in this case. The gap at approximately 47 ms is caused by saturation of the data. Amplitude axis units are arbitrary.

however, that the principle works, and this is an alternative way of reducing ghost cavitation sound, in addition to simply increasing the distance between the subarrays in the source array.

Firing two guns at a delayed time means that the primary signal of the air-gun array is somewhat reduced (corresponding to the primary peak contribution from these two guns). This also means that the amplitude spectrum will also be slightly changed because of this. The amount of change depends on the ratio between the number of guns being used to attenuate the ghost cavitation and the total number of guns in the array.

CAN WE ACTUALLY SEE THE GHOST CAVITATION?

As an attempt to visually observe the ghost cavitation sound, we installed a high-speed camera on one of the source strings. Figure 20 shows a sequence of photos taken at different times after the gun array has fired. We observe part of a weak "cloud" in the upper left of these photos, and we see that this cloud is most visible 16 ms after the source has been fired. When we compare this with the modeling example shown in Figures 6 and 7, we observe that a cavity cloud appearing slightly above the air-gun array (and indeed also above the clustered guns) after approximately 16 ms is indeed very likely. In the photo sequence, the first two guns (to the right in the figure) are single guns, and if we compare the upper right photo in Figure 20 with Figure 6b, we actually observe that the outskirt of the cavity cloud is close to (and above) the two single guns at the tail of the array. According to our acoustical observations, this delay time of 16 ms does not fit exactly with our observed acoustic measurements, where we observe the main burst of high-frequency sound between 8 and 16 ms (see Figure 3) after the source is fired. However, as shown in Figure 21, this time window is actually broader than 8 ms, probably up to 15–16 ms. How much of the signal observed after the main peak (at 45.5 ms) is caused by ghost reflections of the ghost cavitation and how much is caused by direct cavity collapses is hard to judge. Based on simple modeling (that will be discussed in the next section), we find that it is probably a combination of both. Therefore, we conclude that the observed cloud anomaly on the photo sequence, the air-gun modeling examples and the measured acoustic data are consistent, and we confirm the hypothesis that the high-frequency sound is caused by ghost cavitation.

Why do we think that the cavitation collapse is visible on high-speed photographs? One physical effect behind this observation is cavitation luminescence. This is first observed by Marinesco and Trillat (1933). Although the physical effect is the collapse of the cavity, it is also often referred to as sonoluminescence. A comprehensive review of this phenomenon is given by Brenner et al. (2002). In the theory of cavitation luminescence, it is assumed that the temperature inside the cavity reaches values of greater than 5000 K at the final stage of the collapse. Photons are released during this process, which might be observable on high-speed photographs. Another explanation for the observation on the photo is

the simple explanation that what we see is a swarm of cavities (prior to their collapse).

AN ATTEMPT TO MODEL GHOST CAVITATION SOUND

As shown in Figures 6 and 7, we assume that a cavity cloud is formed in the vicinity of the air-gun array. We assume that numerous small cavities are formed within these clouds. The time needed to create a cavity is unknown, but we will assume that this time is very short. This means that we assume that a cavity is "born" instantly because the pressure is below a critical value (that is close to zero). Note that in principle (depending on the design of the air-gun array), there might be several clouds generating numerous cavities. These cavities collapse within a short time according to the formula derived by Rayleigh (1917):

$$T = 0.915R\sqrt{\frac{\rho}{p_h}}, \tag{3}$$

where T is the collapse time for the cavity, R is the initial cavity radius, ρ is the density of water, and p_h is the hydrostatic pressure. If several cavities of various sizes collapse, their collapse time will also vary, and the biggest cavities will collapse at later times according to Rayleigh's equation. Based on the source modeling examples shown in Figures 6 and 7, we assume that the number of cavities (n) and their initial radius (R) have maxima (n_o and R_o, respectively) when the pressure has a minimum and that the modeled pressure is below zero. We therefore assume the following equations for these two parameters:

$$n(t) = n_0\left(1 - \frac{(t-t_0)^2}{t_0^2}\right), \quad \text{for } 0 < t < 2t_0, \tag{4}$$

$$R(t) = R_0\left(1 - \frac{(t-t_0)^2}{t_0^2}\right), \quad \text{for } 0 < t < 2t_0. \tag{5}$$

In equations 4 and 5, we will assume that n and R are zero for $t > 2t_0$. The time $2t_0$ corresponds to the time window, where cavity production is possible, that is when the absolute pressure is modeled to be below zero. An example of n and R as a function of time is shown in Figure 22. Because the two parameters have the same quadratic dependence, the normalized versions are identical. It is reasonable to use a quadratic assumption as suggested in equations 4 and 5 because the lower the pressure is, the higher is the probability for cavity generation. The same argument is valid also for the initial radius of the cavities: It is most likely that the largest cavities are formed when the pressure reaches the minimum value (in our model, that corresponds to $t = t_0$). It should be noted that apart from the modeling example shown in Figures 6 and 7, equations 4 and 5 are phenomenological and are not an attempt to describe the complex physics of cavitation. The nice feature of such a simple model is that it predicts the skew behavior that we observe in the field data: When we assume that the biggest cavities are formed when $t = t_0$, these cavities will have a long collapse time (according to equation 3), whereas cavities created at times longer than t_0 will have a shorter collapse time, and hence we will get an increased number of collapses occurring for the interval $t_0 < t < 2t_0$. A comparison between observed and modeled amplitude of cavitation signal versus time is shown in Figure 23. For this modeling case, we have used $t_0 = 3.5$ ms and $R_0 = 2$ cm. We notice that the modeled response is very similar (but not identical) to the measured signatures. In this example, we have also added the source ghost to the modeled data, assuming reflection coefficients of -0.6 and -0.2, respectively. These rather low numbers are used to account for the fact that we model high-frequency signals. In the modeling, we have assumed that the center of the cavity cloud moves relatively slowly downward, as can be observed from Figures 6 and 7. The physical cause for this vertical motion of the cavity cloud center is that two effects counteract: For shallow depths, the alignment of the ghost signals that occur at the cloud center is weak (the travel paths are different). This alignment improves with cloud depth. The other effect is that the amplitude strength of the ghost signals decreases with cloud depth, causing the cloud center to move slowly (slower than the water velocity) downward with recording time. In the current example, we used a downward cloud velocity of 500 m/s in our simplified modeling. This downward cloud velocity is needed to compute when the ghost signals of the collapsing cavities arrive. We notice from this comparison that it is not easy to recognize the ghost of the ghost cavitation signal in the field data. This might be an indication that the simple one-cloud model used here is not sufficient to model the cavity response. However, we observe that the frequency content of the potential ghost of the ghost cavity signal is weaker for frequencies of greater than 100 kHz (the red curve in Figure 23a) than for lower frequency bands. We think this is caused by a reduction in the magnitude of the sea surface reflection coefficient as frequency is increased (for a more detailed discussion on this issue, see Landrø et al., 2013). Therefore, we think it is reasonable to assume that some of the signal observed after the main peak is caused not only by the ghost of the ghost cavitation, but also from cavities collapsing after the main burst of collapses.

COMPARISON WITH CAVITATION CAUSED BY COLLAPSING BUBBLES

We have seen that it is possible to create high-frequency cavitation sound by single-string arrays. The amplitude level of single-string high-frequency sound is approximately seven to eight times weaker than that of a full array (using a high-pass filter of 10 kHz). Is it possible that the bubble oscillations that occur for all air-gun arrays are strong enough to create some high-frequency cavitation

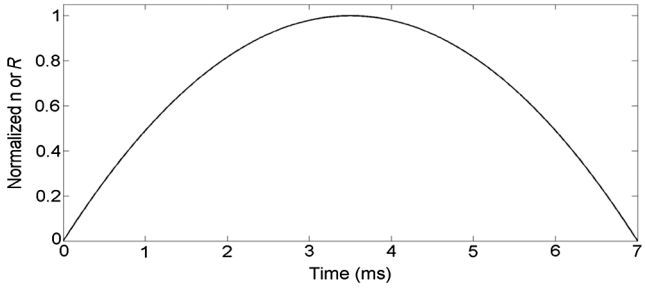

Figure 22. Modeled distributions of number of cavities (n) and initial cavity radius (R) as a function of time. Both distributions are normalized to one, and therefore the two curves are identical: $t_0 =$ 3.5 ms is used in this case.

signal? Figure 24 shows a comparison between the amplitude levels of recorded signatures (after applying a 10 kHz high-pass filter) of a full array using 6.5 m subarray separation distance and 8 m. We clearly see that there is a weak cavitation signal for both configurations. The amplitude strength is approximately 70 times weaker than the cavitation signal created by the primary ghost reflections, but it is clearly observable. We observe the same high-frequency signal also for single subarrays. Hence, it is very likely that this type of cavitation signal is generated by the collapse of individual bubbles and not by any kind of ghost cavitation effects. Although the primary and ghost signals in Figure 24 appear to be nonsaturated and okay, they are actually saturated. Hence, the primary-to-bubble ratio is not correct in Figure 24 because the amplitude of the primary is not correct.

DISCUSSION

Unfortunately, the recorded data in this experiment were saturated. This mainly caused problems for the first strong arrivals, and we have assumed that later and weaker events are not influenced by this. We used visual inspection to judge whether the data were saturated or not. Because the amplitude behavior of the high-frequency signal is very similar to previous measurements (Landrø et al., 2011, 2013), we assume that this error has not damaged the analysis of the high-frequency signal significantly. It is mainly the primary peak and the following ghost that are clipped; however, as can be seen from Figure 3, there is a short sequence (a millisecond duration) of clipping at approximately 44–47 ms. A comparison between the ghost cavitation signal and, for instance, the high-frequency signal created by individual air guns is not possible for this data set due to this saturation. Most of the high-frequency signal created by single air guns occurs immediately after the primary peak, and this part of the signature is lost due to saturation. This is discussed in more detail in the section "High frequencies from a single air gun" in Landrø et al. (2011). All experiments performed in this test confirm the hypothesis of ghost cavitation: The cavitation signal decreases as the subarrays are pulled farther apart from each other, the signal decreases with source depth, and the signal also decreases if the subarrays are shifted or misaligned in the sail line direction to each other (this example is not shown in this paper). Furthermore, if single air guns are fired at a delayed time to the main array (in our case 11 ms), there is an immediate decrease in the high-frequency signal, indicating that the positive signal from the single air gun counteracts the negative ghost reflected signal from all the other guns. The fact that we observe high-frequency signals at greater than 130 kHz is a strong indication that this sound is produced by collapsing cavities.

We find that there are several ways to attenuate the ghost cavitation sound: increasing the width and the length of the air-gun array (meaning that the distance between individual guns is increased), increasing the source depth, and using multilevel sources. Air-gun modeling can also be used to estimate the degree of ghost cavitation. If air-gun modeling shows that there are no negative pressures occurring in the water above the array, this is a strong indication that ghost cavitation will be weak.

How strong is the ghost cavitation signal compared with other sound sources? Figure 25 shows the amplitude spectra normalized to 1 micropascal at 1 Hz and at 1 m. At 1 kHz, the signal is approximately 150 dB, which is comparable or less than typical noise levels from ship traffic. Arvesen and Vendittis (2000) find that the noise level from a 25,000 ton (deadweight) cargo ship at full speed (15.6 knots) is 166 dB at 1 kHz and 156 dB at 10 kHz. Lowering the speed leads to a lowering of the noise level by 10–20 dB. However, we think it is reasonable to assume that ghost cavitation signals from marine air-gun arrays is generally lower or of the same sound level as commercial ship traffic. Kipple (2002) measures the underwater acoustic noise from several cruise ships and finds typical levels at 150 dB for a 10 knot vessel speed at 1 kHz increasing by approximately 10 dB if the speed is increased to 15 knots.

For frequencies greater than 100 kHz, we expect some intrinsic attenuation in the water layer. For 10 kHz, the typical attenuation is 1 dB/km, and the corresponding value for 100 kHz is 30 dB/km. The attenuation of sound in water is dependent on the water temperature, acidity, and salinity. In this experiment, the distance between the source and the hydrophone was between 8 and 11 m, meaning that attenuation effects should be minimal, also for frequencies greater than 100 kHz. In a previous paper (Landrø et al., 2011), the source-hydrophone distance was approximately 50 m, and the ghost cavitation signals for this experiment and that discussed in the 2011 paper are very similar. We have not made any attempts to estimate the attenuation of sound in water based on these two experiments so far.

The amount and strength of the ghost cavitation signal are dependent of the sea surface reflection coefficient, as shown in Figure 13 in Landrø et al. (2013). However because a major part of the energy

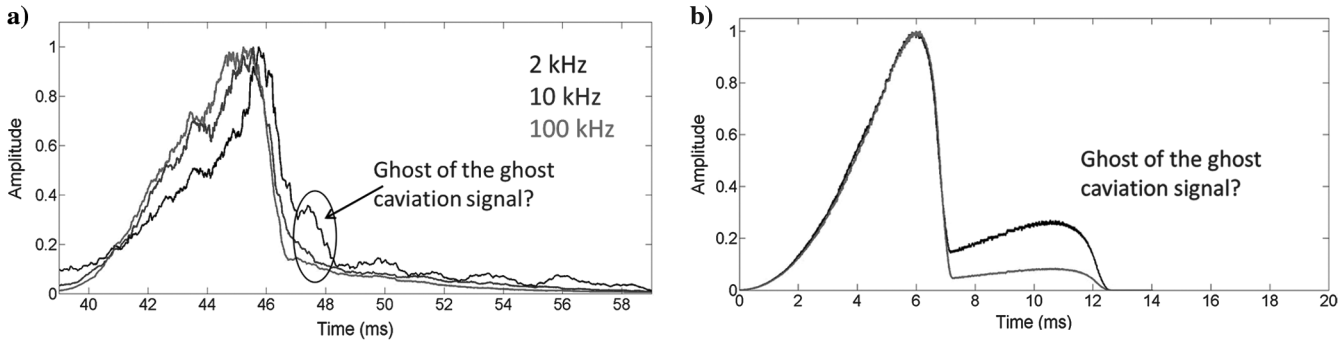

Figure 23. Comparison of ghost cavitation amplitude (after absolute value and smoothing) for (a) full source (9 m depth and 6.5 m separation distance) and (b) modeled amplitude response. (a) The black curve represents 2 kHz high pass, the dark gray 10 kHz, and the light gray 100 kHz high pass. For the right figure, the black curve represents a reflection coefficient of −0.6 and the gray curve −0.2. In the modeling, $t_0 = 3.5$ ms. All curves are normalized to their maximum peaks.

emitted by an air gun is of relatively low frequency (20–50 Hz), it is not very likely that the reflection coefficient is significantly different from −1 for this frequency band, as shown in Figure 20 in Landrø et al. (2013).

Will ghost cavitation signals be a prominent part of the high-frequency signals emitted by air-gun arrays also when the water surface is covered by ice, as for instance in arctic areas? In this case, the "effective" reflection coefficient of the free surface is practically unchanged, as shown in Appendix A. This means that the amount of cavity creation will be practically the same if an air-gun array is fired in water covered by ice. For higher frequencies, the actual shape of the bottom of the ice will influence the scattered wavefield, an effect similar to a nonsmooth water-air surface. We have also assumed that the ice is nonporous and homogeneous in this case. Yamamoto and Badiey (1986) discuss an example in which they estimate the reflection coefficient for inhomogeneous transversely isotropic porous sea ice. For angles of incidence less than 10°, they find that the absolute value of the reflection coefficient is practically equal to 1 for frequencies of 0.5, 1.0, and 3.0 kHz.

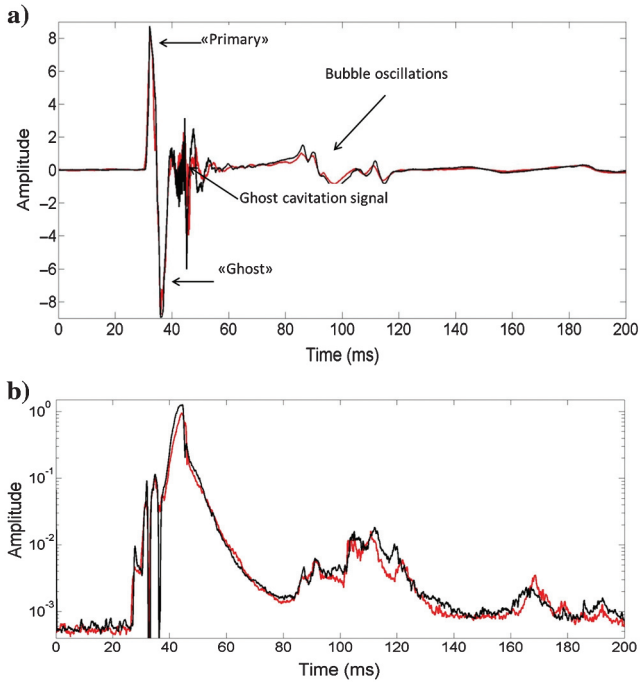

Figure 24. (a) Stack of unfiltered shot records for full array using 6.5 m separation distance (black) and 8 m (red). (b) Envelope after 10 kHz high-pass filtering, absolute value, and smoothing. The source depth is 9 m. The 16 shots have been stacked for both cases. The ghost cavitation signal (42 ms) is approximately 70 times stronger than the corresponding signal associated with the bubble collapse (between 90 and 125 ms). The hydrophone is located at 17 m depth. Note that the signals annotated as "primary" and "ghost" in the top figure are saturated, and hence the amplitude values of these are not correct.

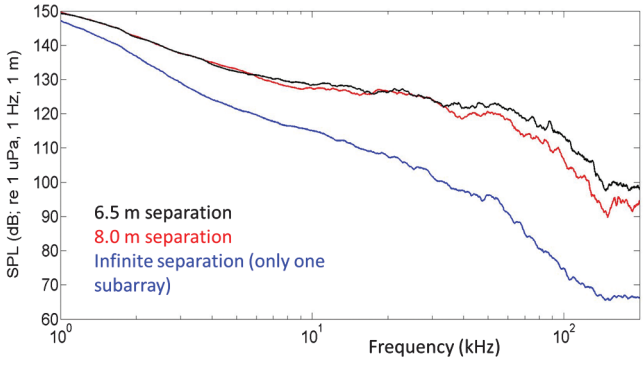

Figure 25. Amplitude spectra of two subarrays separated by 6.5 m (black), 8 m (red), and one subarray only (blue). Notice that the slope is steeper for the single array. It is assumed that the cavities collapse 14 m away from the hydrophone.

CONCLUSION

For compact air-gun arrays, we suggest that the ghost reflections could create "cavity clouds" around the array, first above the air-gun array, and at a later stage also below the array. We refer to this phenomenon as ghost cavitation. These cavities create high-frequency sound at the collapse, and are one of the major causes for the high-frequency signals (more than 10 kHz) generated by marine air-gun arrays. We find that the amount and strength of this high-frequency signal decrease if the separation distance between the subarrays is increased. Also, single subarrays may create a ghost cavitation sound, although it is weaker in signal strength compared with full arrays. The amount of ghost cavitation decreases with increasing the source depth. The sea state and especially the shape of the sea surface influence the ghost cavitation. Firing single air guns at a delayed time to counteract the ghost cavitation lead to less high-frequency sound. The actual delay for this type of attenuation is critical. High-speed photos show a cloud anomaly that is consistent with air-gun source modeling and the acoustic-field measurements. For an air-gun array consisting of two subarrays separated by 6.5 m and fired at 9 m depth, we find that the high-frequency signals emitted between 1 and 10 kHz are of the same strength or weaker compared with conventional cargo ships, depending on their size and speed.

ACKNOWLEDGMENTS

We want to thank Statoil and CGG for permission to present the results and for funding the experiments presented in this paper. M. Landrø thanks the Norwegian Research Council for financial support to the ROSE Consortium at NTNU and the Research Centre for Arctic Petroleum Exploration Consortium for support. Furthermore, he thanks the Geophysics Department at Colorado School of Mines for hosting him during the autumn semester of 2014. Finally, we want to thank the associate editor and the reviewers for numerous valuable comments and suggestions.

APPENDIX A

REFLECTION COEFFICIENT FOR ICE LAYER

In arctic areas, the water is often covered by ice. The thickness of the ice layer might vary between 0 and 5 m (Laxon et al., 2003). The effective reflection coefficient for a seismic wave being reflected from a water surface covered by a thin ice layer is given by (Brekhovskikh and Godin, 1998)

$$R_{\text{eff}} = \frac{r_1 + r_2 e^{i\varphi}}{1 + r_1 r_2 e^{i\varphi}}, \tag{A-1}$$

where r_1 and r_2 are the reflection coefficients for water-ice and ice-air, respectively. The phase term is given as

$$\varphi = \frac{2\omega z}{v_{\text{ice}}} \tag{A-2}$$

where ω is the circular frequency, z is the thickness of the ice layer, and v_{ice} is the P-wave velocity in ice. For simplicity, we have assumed horizontal layers and zero incidence waves in the above equations. The absolute value of the effective reflection coefficient (equation A-1) is equal to

$$|R_{\text{eff}}| = \sqrt{\frac{r_1^2 + r_2^2 + 2r_1 r_2 \cos\varphi}{1 + r_1^2 r_2^2 + 2r_1 r_2 \cos\varphi}} \tag{A-3}$$

The water-ice reflection coefficient is approximately equal to 0.4 ($r_1 = 0.4$), and the ice-air reflection coefficient is very close to -1 ($r_2 = -1$). This means that the absolute value of the effective reflection coefficient (including tuning effects) is very close to 1. Hence, we conclude that the effect of an ice cover does not change the mechanism for cavity creation significantly.

REFERENCES

Aizenberg, M., I. Tsvankin, A. Aizenberg, and B. Ursin, 2008, Effective reflection coefficients for curved interfaces in TI media: 70th Annual International Conference and Exhibition, EAGE, Extended Abstracts, P346.

Amundsen, A., and M. Landrø, 2010, Seismic sources. Part V: The hearing of marine mammals: GeoExpro, **7**, 64–66.

Arvesen, P. T., and D. J. Vendittis, 2000, Radiated noise characteristics of a modern cargo ship: Journal of the Acoustical Society of America, **107**, 118–129, doi: 10.1121/1.428344.

Breitzke, M., O. Boebel, S. El Naggar, W. Jokat, and B. Werner, 2008, Broad-band calibration of marine seismic sources used by R/V Polarstern for academic research in polar regions: Geophysical Journal International, **174**, 505–524, doi: 10.1111/j.1365-246X.2008.03831.x.

Brekhovskikh, L. M., and O. A. Godin, 1998, Acoustics of layered media I: Springer.

Brenner, M. P., S. Hilgenfeldt, and D. Lohse, 2002, Single-bubble sonoluminescence: Reviews of Modern Physics, **74**, 425–484, doi: 10.1103/RevModPhys.74.425.

Ceccio, S. L., and C. E. Brennen, 1991, Observations of the dynamics and acoustics of travelling bubble cavitation: Journal of Fluid Mechanics, **233**, 633–660, doi: 10.1017/S0022112091000630.

Coste, E., D. Gerez, H. Groenaas, J. F. Hopperstad, O. P. Larsen, R. Laws, J. Norton, and M. Padula, 2014, Attenuated high-frequency emission from a new design of air-gun: 84th Annual International Meeting, SEG, Expanded Abstracts, 132–137.

Goold, J. C., and P. J. Fish, 1998, Broadband spectra of seismic survey air-gun emissions, with reference to dolphin auditory thresholds: Journal of the Acoustical Society of America, **103**, 2177–2184, doi: 10.1121/1.421363.

Groenaas, H. S. G., S. A. Frivik, A. S. Melboe, and M. Svendsen, 2011, A novel marine mammal monitoring system utilizing the seismic streamer spread: 73rd Annual International Conference and Exhibition, EAGE, Extended Abstracts, D047.

Kipple, B., 2002, Southeast Alaska cruise ship underwater acoustic noise: Technical Report No. NSWCCD-71-TR-2002/S74, Naval Surface Warfare Center, 39.

Landrø, M., 1992, Modelling of GI gun signatures: Geophysical Prospecting, **40**, 721–747, doi: 10.1111/j.1365-2478.1992.tb00549.x.

Landrø, M., 2000, Source signature determination by inversion of minisstreamer data: The Leading Edge, **19**, 46–49, doi: 10.1190/1.1438452.

Landrø, M., L. Amundsen, and D. Barker, 2011, High-frequency signals from air-gun arrays: Geophysics, **76**, no. 4, Q19–Q27, doi: 10.1190/1.3590215.

Landrø, M., L. Amundsen, and J. Langhammer, 2013, Repeatability issues of high-frequency signals emitted by air-gun arrays: Geophysics, **78**, no. 6, P19–P27, doi: 10.1190/geo2013-0142.1.

Landrø, M., S. Strandenes, and S. Vaage, 1991, Use of near-field measurements to compute far-field marine source signatures — Evaluation of the method: First Break, **9**, 375–385.

Landrø, M., G. Zaalberg-Metselaar, B. Owren, and S. Vaage, 1993, Modeling of water-gun signatures: Geophysics, **58**, 101–109, doi: 10.1190/1.1443339.

Laws, R. M., 2012, Cetacean hearing-damage zones around a seismic source, *in* A. N. Popper, and A. Hawkins, eds., The effects of noise on aquatic life: Springer Science + Business Media, LLC, 473–476, doi: 10.1007/978-1-4419-7311-5_107.

Laxon, S., N. Peacock, and D. Smith, 2003, High interannual variability of sea ice thickness in the Arctic region: Nature, **425**, 947–950, doi: 10.1038/nature02050.

Marinesco, N., and J. J. Trillat, 1933, Action des ultrasons sur les plaques photographiques: Proceedings of the Royal Academy of Science, Amsterdam, **196**, 858–860.

Parkes, G., A. M. Ziolkowski, L. Hatton, and T. Haugland, 1984, The signature of an airgun array: Computation from near-field measurements including interactions — Practical considerations: Geophysics, **49**, 105–111, doi: 10.1190/1.1441640.

Rayleigh, O. M., 1917, On the pressure developed in a liquid during the collapse of a spherical cavity: Philosophical Magazine, **34**, 94–98, doi: 10.1080/14786440808635681.

Southall, B. L., A. E. Bowles, W. T. Ellison, J. J. Finneran, R. L. Gentry, C. R. Greene Jr., D. Kastak, D. R. Ketten, J. H. Miller, P. E. Nachtigall, W. J. Richardson, J. A. Thomas, and L. Tyack, 2007, Marine mammal noise exposure criteria: Initial scientific recommendations: Aquatic Mammals, **33**, 411–521, doi: 10.1578/AM.33.4.2007.411.

Yamamoto, T., and M. Badiey, 1986, Propagator matrix for acoustic wave propagation through anisotropic porous media, *in* T. Akal, and J. M. Berkson, eds., Ocean seismo-acoustics: Low-frequency underwater acoustics: Springer-Verlag, 463–472, doi: 10.1007/978-1-4613-2201-6_45.

Ziolkowski, A. M., 1970, A method for calculating the output pressure waveform from an air gun: Geophysical Journal of the Royal Astronomical Society, **21**, 137–161, doi: 10.1111/j.1365-246X.1970.tb01773.x.

Ziolkowski, A. M., G. Parkes, L. Hatton, and T. Haugland, 1982, The signature of an air gun array: Computation from near-field measurements including interactions: Geophysics, **47**, 1413–1421, doi: 10.1190/1.1441289.